Multifractal conductance fluctuations in high-mobility graphene in the Integer Quantum Hall regime

Kazi Rafsanjani Amin,[1,2] Ramya Nagarajan,[1] Rahul Pandit,[1] and Aveek Bid[1,*]

[1] *Department of Physics, Indian Institute of Science, Bangalore, Karnataka, India 560012*

[2] *Current address: Department of Microtechnology and Nanoscience, Chalmers University of Technology, 412 96 Gothenburg, Sweden*

We present the first experimental evidence for the multifractality of a transport property at a topological phase transition. In particular, we show that conductance fluctuations display multifractality at the integer-quantum-Hall $\nu = 1 \longleftrightarrow \nu = 2$ plateau-to-plateau transition in a high-mobility mesoscopic graphene device. We establish that to observe this multifractality, it is crucial to work with very high-mobility devices with a well-defined critical point. This multifractality gets rapidly suppressed as the chemical potential moves away from these critical points. Our combination of multifractal analysis with state-of-the-art transport measurements at a topological phase transition provides a novel method for probing such phase transitions in mesoscopic devices.

Since its discovery, the integer quantum Hall (IQH) effect, a continuous quantum-phase transition in a two-dimensional electron gas (2DEG)[1], has provided us with a paradigm for topological phase transitions. In the presence of a large magnetic field B, applied perpendicular to the surface, the density of states (DOS) of a non-interacting 2DEG breaks into discrete, quantized Landau levels. Disorder broadens these degenerate Landau levels into bands of extended states that are separated by localized states. When the Fermi level $\mathrm{E_F}$, which we can tune by changing either B or the charge-carrier density n, lies in the part of the spectrum with localized states (cf. Fig. 1(a)), the Hall conductance G_{XY} is quantized in units of e^2/h, and the transverse conductance G_{XX} becomes vanishingly small, with $G_{XX} = 0$ at temperature $T = 0$ [2]. In this regime, transport takes place through chiral edge modes, whose number is dictated by the topological Chern number of the system [3–6]. If, by contrast, $\mathrm{E_F}$ lies in the range of energies at the center of the Landau levels with extended states, transport proceeds through the bulk with $G_{XX} \neq 0$ and a non-quantized G_{XY}. The localization-delocalization transition occurs in a 2DEG in the IQH regime as the system crosses the mobility edge, which separates localized and extended states [7–10]. The eigenstates at the mobility edge are *critical* and different from both localized and extended states [7]. As the Landau-level filling factor ν approaches its critical value, the localization length ξ diverges algebraically as $\xi \propto |\nu - \nu_C|^{-\gamma}$. Theoretical studies have shown that observables like the distribution of the local density $|\psi(\mathbf{r})|^2$ [7, 11] or the equilibrium current density $|j(\mathbf{r})|^2$ [12] display multifractality of the density fluctuations that leads to anomalous diffusion [10] and, consequently, a power-law decay of the density correlations, a slow decay of temporal wave-packet auto-correlations [13] and, most significantly for our purpose, multifractal conductance fluctuations [14–18].

In this Letter, we present the first experimental evidence for the multifractality of a transport property at a topological phase transition [3–6]. In particular, we show that, in high-mobility-graphene at the first IQH plateau-to-plateau transition, the conductance shows multifractal fluctuations as a function of ν.

Multifractality was initially introduced to characterize the statistical properties of fluid turbulence [19, 20] and thereafter studied, not only in turbulent flows [21–23], but also in a variety of fields like the analysis of DNA sequences [24], atmospheric science [25, 26], econophysics [27], heartbeat dynamics [28, 29], and cloud structure [30], and many other parts of physics. In condensed-matter science, most investigations of multifractality, which manifests itself at some phase transitions, employ a combination of theoretical and numerical techniques [15–17, 31–35]. The experimental characterizations of multifractality in such condensed-matter settings require high-precision experiments in good-quality samples, often at low temperatures and at high magnetic fields. Two recent examples of such measurements are the study of multifractal conductance fluctuations at low magnetic fields [14] and the study of multifractal superconductivity in the weak-disorder regime [36, 37]. By using high-mobility-graphene and tuning ν, we demonstrate that conductance fluctuations display multifractality in the vicinity of the first IQH plateau-to-plateau transition.

Our electrical-transport measurements were carried out on hexagonal-boron-nitride (hBN) encapsulated graphene devices with one-dimensional ohmic contacts (details in Supplemental Materials). The electrical transport measurements were carried out in a dilution refrigerator, with a base temperature of 20 mK, by using low-frequency lock-in-measurement techniques in a multi-probe configuration at a low bias current ($\leq$1 nA) to avoid Joule heating. We focus on our data from a particular bilayer-graphene device, 1DC8. This sample was thermally cycled multiple times; the data we present did not change significantly after this thermal cycling.

In Fig. 1(c), we present plots of the longitudinal resistance R versus the back-gate voltage V_G, measured at $B = 0$

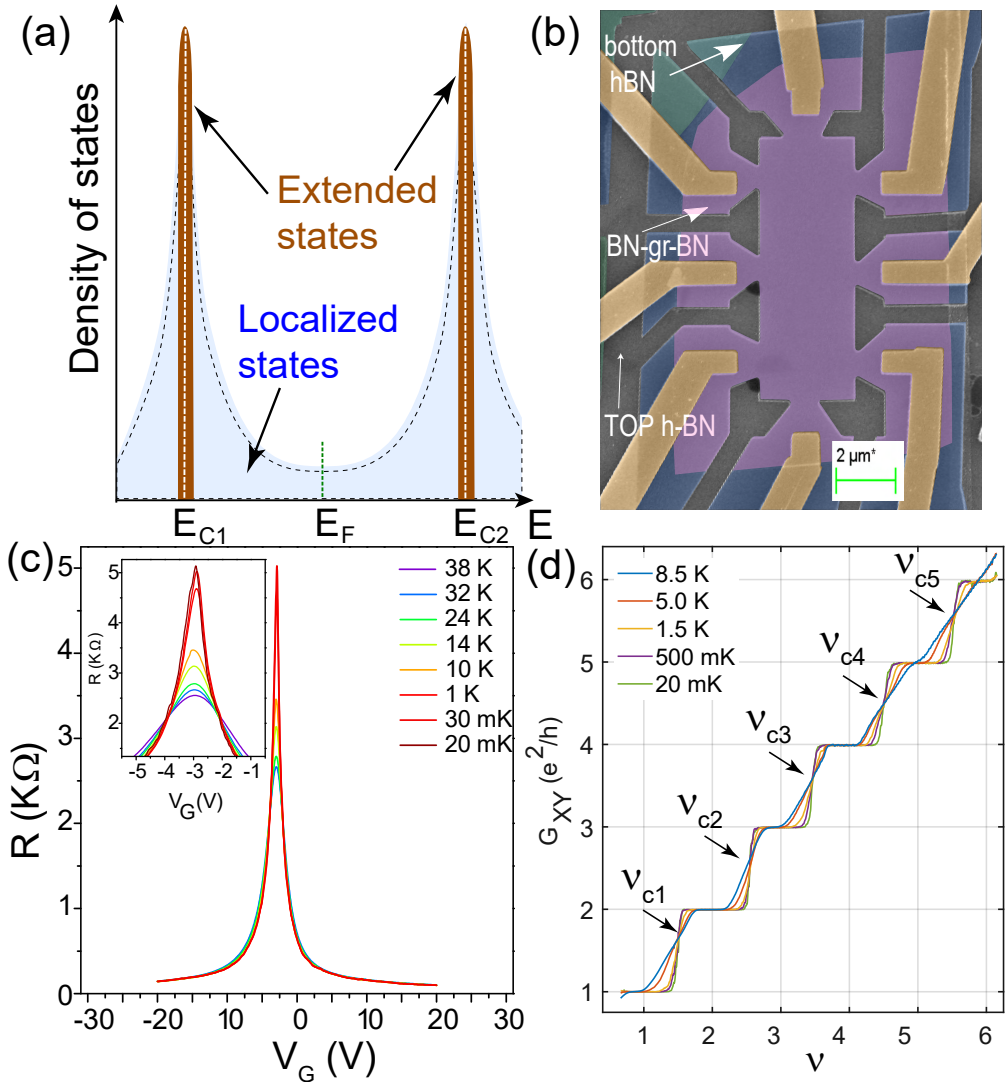

FIG. 1. (a) A schematic diagram illustrating the dependence of the density of states (DOS) of the 2DEG on energy in the IQH regime, showing brown regions with extended states, at the centers of the disorder-broadened Landau levels, separated by light-blue regions with localized states. Plateaux in the Hall conductance are observed when the Fermi energy E_F (green dashed line) lies deep within the band of localized states. The quantum phase transitions between the localized and extended states occur at the mobility edge around the critical energies E_{C1} and E_{C2}. (b) A false-color SEM image of our device 1DC8 (see text). (c) Plots showing the dependence of R on V_G at different temperatures. The measurements were carried out at $B = 0$ T. The inset shows a zoomed-in plot near the Dirac point. (d) Plots of G_{XY} versus the filling factor ν measured at different temperatures and magnetic field $B = 16$ T. The arrows mark the positions of the IQH critical points at which the localization-delocalization transitions occur.

and different values of T. With the charge-neutrality or Dirac point at $V_D = -2.91$ V, we find that R is as low as 30 Ω at $V_G \simeq 30$ V. The field-effect mobility, estimated at $T = 20$ mK, is $\mu = 1,28,000$ cm^{2}V^{-1}s^{-1}. In the inset of Fig. 1(c), we show magnified plots of R versus V_G near the Dirac point. Close to the Dirac point ($|\Delta V_G| = |V_G - V_D| \leq 1$ V), we observe that R increases with decreasing T; this suggests an insulating state. However, for $|\Delta V_G| \geq 1$ V, R decreases with decreasing T, indicating metallic behavior. Clearly, the effect of impurity scattering is significantly suppressed in our sample; indeed, this is a precondition for observing the number-density-induced insulator-metal transition in graphene [38].

Figure 1(d) shows plots versus $\nu(= nh/eB)$ of G_{XY}, in units of e^2/h, from our measurements at different temperatures T and at $B = 16$ T. If we focus on the plot for T=20 mK, we observe well-developed plateaux in G_{XY} at all integer multiples of e^2/h, indicating a complete lifting of the layer, spin, and valley degeneracies of the Landau-level

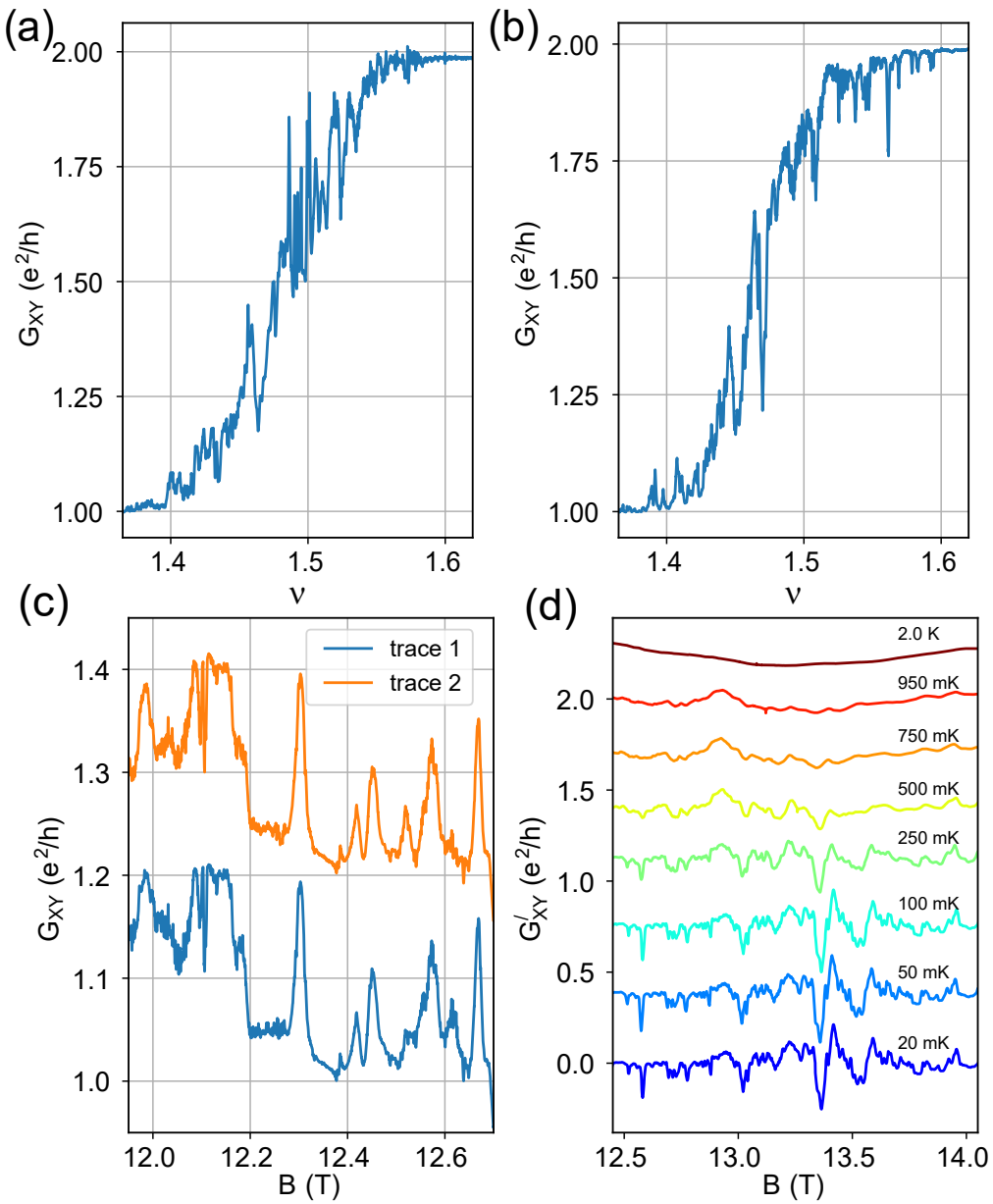

FIG. 2. Plots of G_{XY} versus ν measured during the transition from $\nu = 1$ to $\nu = 2$ at (a) fixed value of the magnetic field $B = 16$ T and (b) a fixed number density $n = 4.75 \times 10^{11}$ cm^{-2}. (c) Plots of two different traces of G_{XY} versus B, measured between $\nu = 1.64$ and $\nu = 1.54$, showing the reproducibility of the mesoscopic conductance fluctuations. These data sets have been shifted vertically for clarity. (d) Plots of segments of data of G'_{XY} (Eq. 1) versus B, for the $\nu = 1 \longleftrightarrow \nu = 2$ transition, measured at different temperatures T and at a fixed carrier density $n = 4.75 \times 10^{11}$ cm^{-2}. Reproducible oscillations are observed over a wide temperature ranger; the amplitude of these oscillations decreases with increasing T. The data sets have been shifted vertically for clarity. The data presented in (c) are from a different cool-down cycle than those in (a), (b), and (d).

spectra [39, 40]. For any one of the transitions between two adjacent plateaux, the plots of G_{XY} versus ν, measured at different temperatures, intersect at a point, in the (ν, G_{XY}) plane. We identify each such intersection as a critical point: (ν_{Ci}, $G_{XY_{Ci}}$), with i a positive integer, is the critical point for the $i \rightarrow (i+1)$ plateau-to-plateau quantum phase transitions from localized to delocalized states [8].

We now focus on the mesoscopic conductance fluctuations in the vicinity of these critical points. In Figs. 2(a-b), we show plots of G_{XY} versus ν, for the $\nu = 1 \longleftrightarrow \nu = 2$ quantum-Hall transition, measured at $T = 20$ mK. We tune ν either by changing n, at $B = 16$ T (Fig. 2(a)), or by changing B, at $n = 4.75 \times 10^{11}$ cm^{-2} (Fig. 2(b)). These

plots show that G_{XY} has significant fluctuations across the plateau-to-plateau transition. In Fig. 2(c), we present plots of two traces of G_{XY} measured at $T = 20$ mK – these data sets have been shifted vertically for clarity. The fluctuation profiles are the same in the two traces; this establishes that they are mesoscopic fluctuations with a unique magnetofingerprint. These fluctuations remain reproducible over a particular thermal cycle; however, the detailed profile changes if we thermally cycle the device to $T > 10$ K and back.

We obtain the conductance fluctuations $G'_{\Box}(x)$ from these measurements by subtracting a smooth background from the measured data as follows:

$$G'_{\Box}(x) = G_{\Box}(x) - F[G_{\Box}(x)]. \tag{1}$$

In Eq. 1, x can be B or V_G, $G_{\Box}$ stands for G_{XX} or G_{XY}, and the function $F[G_{\Box}(x)]$ is the smooth background in $G_{\Box}(x)$ (see the Supplemental Material). In Fig. 2(d), we show representative plots of G'_{XY} versus B, from our measurements at the plateau-to-plateau transition $\nu = 1 \longleftrightarrow \nu = 2$, for different values of T and at a fixed value of $n = 4.75 \times 10^{11}$ cm^{-2}. As we increase T, the mean amplitude of the fluctuations in G'_{XY} decreases, but the plots of G'_{XY} retain their principal features because of the magnetofingerprint of mesoscopic fluctuations; these features go away finally below the measurement-noise level for $T > 1$ K. Although these fluctuations in G'_{XY} disappear for $T > 1$ K, the plateaux of G_{XY}, at e^2/h and $2e^2/h$, survive until much higher temperatures [Fig. 1(b)]. Thus, the disappearance of these conductance fluctuations is not a consequence of the disappearance of the quantum-Hall effect because of thermally induced level broadening.

Having established the mesoscopic origin of the fluctuations in the conductance across the plateau-to-plateau transitions, we now analyze the multiscaling behavior and statistics of the fluctuations in the vicinity of the $\nu = 1 \longleftrightarrow \nu = 2$ critical point. Our multifractal analysis of these fluctuations is akin to the analysis in our low-field study of universal conductance fluctuations in single-layer graphene [14] (for details of the analysis, see the Supplementary Material). Briefly, we divide the G'_{XY} data-series into several segments, each centered at different values of the filling factor ν, and we compute the multifractal spectrum as follows. We detrend each such segment and sub-divide it into N_s overlapping segments, indexed by j, and containing s data points, with $1 \leq j \leq N_s$. We obtain the generalized Hurst exponents $h(q)$ from the power-law-scaling behavior of the order-q moment of the fluctuations $F_q(s)$ by using the following relations:

$$g_{rms}(j) = \left[\frac{1}{s}\sum_{i=1}^{s}(g_i)^2\right]^{1/2}; \tag{2}$$

$$F_q(s) = \left[\frac{1}{N_s}\sum_{j=1}^{N_s} g_{rms}(j)^q\right]^{1/q} \sim s^{h(q)}. \tag{3}$$

We obtain $h(q)$ for a range of values of q. A q-dependent $h(q)$ indicates multifractality. As an example, in Fig. 3(a), we show representative plots of $\log[F_q(s)]$ versus $\log[s]$, from one of our data-series for G'_{XY}, for $q = \pm 4$; the circles represent the data-points, and the thick lines are linear fits to the data. The difference in the slopes of the plots suggest that $h(-4) > h(4)$; this is borne out by the plot of $h(q)$ in Fig. 3(b), for $-4 \leq q \leq 4$.

Multifractality can be represented by the singularity spectrum, which is a plot of $f(\alpha)$ versus α; this is obtained by the Legendre transformation of $h(q)$ as follows:

$$\begin{aligned} \alpha &= h(q) + qh'(q); \\ f(\alpha) &= q[\alpha - h(q)] + 1 \end{aligned} \tag{4}$$

In Fig. 3(c), we show a plot of $f(\alpha)$, obtained at 20 mK near the $\nu = 1 \longleftrightarrow \nu = 2$ critical point. The width of $f(\alpha)$, in Fig. 3(c), is $\Delta\alpha \simeq 1.1$. This indicates significant multifractality of the conductance fluctuations at this plateau-to-plateau transition. The maximum of $f(\alpha)$ is located at $\alpha_0 = 2.21$ (marked by an arrow in the figure), with $f(\alpha_0) = 1$. The maximum of $f(\alpha)$ provides the support dimension, of the data series, which is one here. In the Supplementary Material, we show the standard deviations of the small-amplitude fluctuations that we analyze; they are at least ten times more than the noise level measured at the $\nu = 1$ plateau. Hence, our plot of $f(\alpha)$ is not contaminated significantly by measurement noise.

We note that $f(\alpha_0)$ is asymmetrical around α_0. To understand the origin of this asymmetry, recall that, in the Legendre transformation [Eq. 4], the regions $q > 0$ and $q < 0$ map, respectively, onto the $\alpha < \alpha_0$ and $\alpha > \alpha_0$ regions of the spectrum. Hence, because of the summation procedure involved in computing $h(q)$ [Eq. 3], small-amplitude

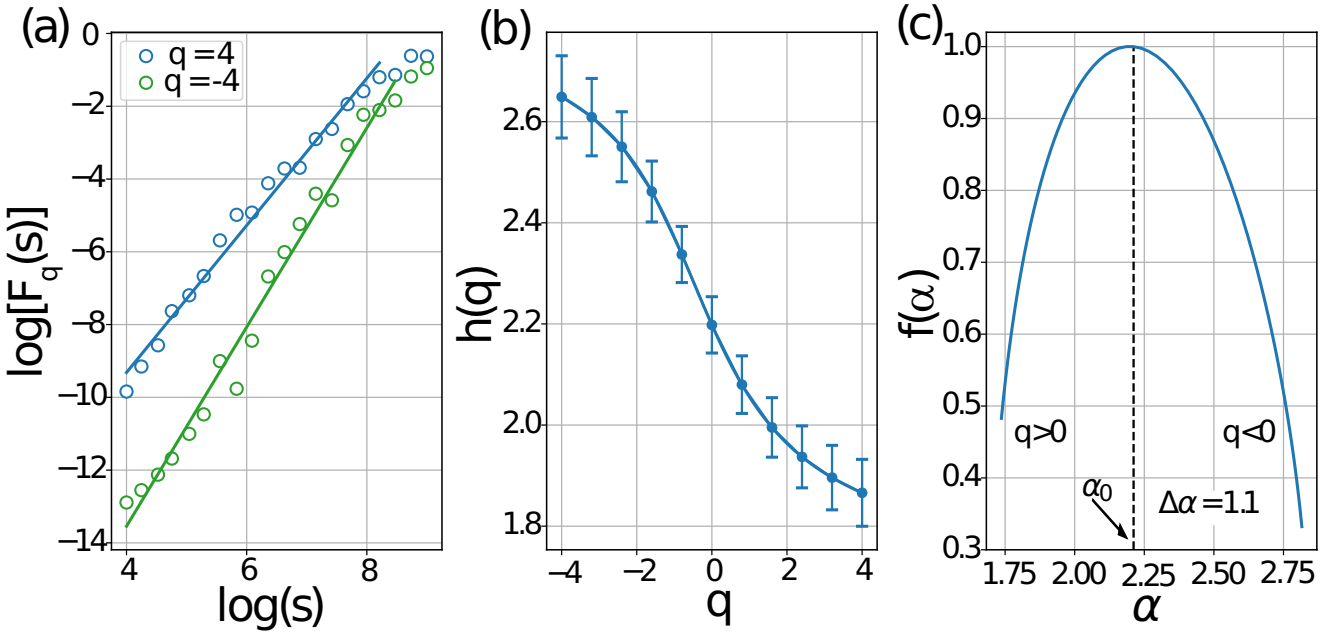

FIG. 3. (a) Plots of $\log[F_q(s)]$ versus $\log[s]$ (see Eq. 3), for $q = -4$ (blue circles) and $q = 4$ (green circles) for a typical data-segment of G'_{XY}. The thick lines are the linear fits to the data points. (b) Plot of $h(q)$ (see Eq. 3) versus q for the data-segment shown in (a). (c) Plot of the singularity spectrum $f(\alpha)$ versus α (see Eq. 4) that we obtain from (b). The maximum value of this spectrum is $f_{max}(\alpha) = 1$; this is located at $\alpha_0 \simeq 2.21$ (marked by an arrow). These data were obtained at $\nu = 1.47$ and 20 mK.

fluctuations in G'_{XY} dominate the $\alpha > \alpha_0$ part of $f(\alpha)$, whereas large-amplitude fluctuations in G'_{XY} dominate the $\alpha < \alpha_0$ part. This asymmetry of $f(\alpha)$ suggests, therefore, a difference between the correlations for small- and large-amplitude fluctuations.

We have also obtained the singularity spectra from plots of G_{XY} versus V_G at $B = 16.0$ T and $T = 20$ mK in the vicinity of the $\nu = 1 \longleftrightarrow \nu = 2$ transition (cf. Fig. S1(b)). We obtain the spectral width $\Delta\alpha$ and plot it in Fig. 4(a) versus $\nu - \nu_C$. At $|\nu - \nu_C| = 0$, $\Delta\alpha \simeq 1.3$, which decreases sharply to $\Delta\alpha \sim 0.2$ at $|\nu - \nu_C| \sim 0.15$. The peak in $\Delta\alpha$ at $\nu \simeq \nu_C$ implies that the multifractality in G_{XY} increases sharply near the $\nu = 1 \longleftrightarrow \nu = 2$ plateau-to-plateau critical point. The maximum of $\Delta\alpha$ lies within the error bars of our determination of ν_C from the crossing points in Fig. 1(d).

The plot of $\Delta\alpha$ versus ν has a small but finite width away from $\nu = \nu_C$; this indicates that G_{XY} displays multifractality not only at this IQH critical point but also in a region around $\nu = \nu_C$. We note that the critical states are confined to $E = E_C$ only in the thermodynamic limit. For a finite system, all states with localization length ξ larger than the system size appear to be extended, and the distribution of physical observables (including conductance fluctuations) is multifractal [41]. The divergence of ξ, away from $\nu = \nu_C$, is suppressed only algebraically, and is governed by γ; so the critical states, for a finite-sized system can be observed away from ν_C, with algebraically reduced probability. Thus, our observation of a finite amount of multifractality away from critical point ν_C can be attributed to finite-size effects.

In Fig. 4(b) we plot $\Delta\alpha$ versus T. We note that $\Delta\alpha$ reduces from $\simeq 1.4$ to less than 0.2 as T increases from 100 mK to 1.0 K. To understand this T dependence of $\Delta\alpha$, note that the effects of quantum-interference-induced localization-delocalization is most prominent at low temperatures. As the T increases, decoherence induced by inelastic thermal scattering reduces quantum interference and results in delocalization [42]. Thus, the multifractality we observe at the $\nu = 1 \longleftrightarrow \nu = 2$ transition is expected to disappear with increasing T. As we have mentioned earlier, this multifractality of the fluctuations in G_{XY} decreases well before the IQH plateaux disappear.

Earlier studies on high-mobility GaAs/AlGaAs heterostructures mesoscopic samples have shown that the integer quantum Hall transitions are accompanied by large, reproducible fluctuations in both G_{XX} and G_{XY} as functions of B and n [43–45]. The amplitudes of these fluctuations grow as the size of the sample is reduced. Despite an expectation that multifractal analysis of these fluctuations is essential for a complete description of the criticality in the IQH regime [7, 13], in particular, and for topological phase transitions in general, experimental confirmation of

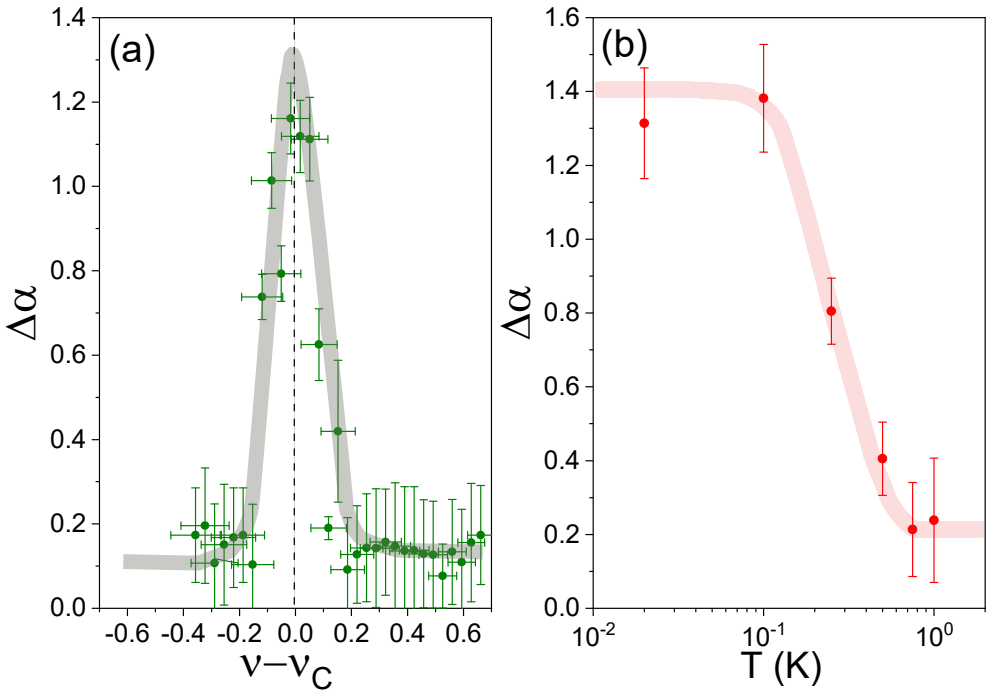

FIG. 4. (a) Plot of the spectral width $\Delta\alpha$ versus $\nu - \nu_C$ for the device B15D4. The vertical line marks the $\nu = 1 \longleftrightarrow \nu = 2$ critical point. The gray-shaded curve is a guide to the eye. The error bars for the $\nu - \nu_C$-axis are calculated from the the intrinsic impurity level in the device; the error bars in the $\Delta\alpha$ axis are derived from the error in calculating the slopes of the plots of $\log[F_q(s)]$ versus $\log[s]$. (b) Plot of $\Delta\alpha$ versus T for the device 1DC8, at a fixed value $\nu - \nu_c = 0.1$ across the $\nu = 1 \longleftrightarrow \nu = 2$ plateau-to-plateau transition. The red-shaded curve is a guide to the eye.

this multifractality has been missing hitherto.

We have presented the first experimental evidence for the multifractality of a transport property at a topological phase transition [3–6]. Our combination of multifractal analysis with state-of-the-art transport measurements at a topological phase transition provide a novel method for probing topological phase transitions in mesoscopic devices. And our study resolves an outstanding question in nanoscale devices, namely, the multifractality of conductance fluctuations at such transitions in a high-mobility 2DEG. In particular, we have shown that conductance fluctuations display multifractality at the integer-quantum-Hall $\nu = 1 \longleftrightarrow \nu = 2$ plateau-to-plateau transition in a high-mobility mesoscopic graphene device. At this transition, we have demonstrated reproducible mesoscopic fluctuations in G_{XY} (see the Supplemental Material), with clear multifractal spectra. This multifractality gets rapidly suppressed as ν moves away from ν_C or as T is increased. We have established that, to observe this multifractality, it is crucial to work with very high-mobility devices, with a well-defined critical point. Our results show that the multiscaling of conductance fluctuations provide a new and clear signature for the IQH $\nu = 1 \longleftrightarrow \nu = 2$ plateau-to-plateau transition. Although theoretical studies have shown the multifractality of eigenfunctions at this transition (see, e.g., Ref. [7, 41, 43, 46–48]), there has been no study hitherto of the multifractality of transport coefficients here. We conjecture that similar multifractality of conductance fluctuations should also be present in (a) all IQH plateau-to-plateau transitions, (b) the fractional-Quantum-Hall transitions, and (c) in single-layer graphene devices. Our preliminary results support the conjectures (a) and (c).

We than S.S. Ray for fruitful discussions. AB acknowledges funding from DST (DST/SJF/PSA-01/2016-17). KRA thanks CSIR, MHRD, Govt. of India for financial support. RN thanks MHRD, Govt. of India, for financial support. The authors thank NNfC, CeNSE, IISc for the device fabrication facilities and MNCF, CeNSE, IISc for the device characterization facilities. RP acknowledges support from CSIR, SERB, and the National Supercomputing Mission (India).

SUPPLEMENTARY MATERIALS

Appendix A: Characteristics of the device B15D4

In Fig. S1, we present the characteristics of the device B15D4. Fig. S1(a) shows a plot of the resistance measured as a function of the gate voltage at $T = 20$ mK. The Dirac point is located at $V_D = -0.22$ V. Fig. S1(b) shows the quantum Hall plateau $\nu = 1$ to $\nu = 2$ transition obtained by sweeping the gate voltage at $T = 20$ mK and $B = 16$ T.

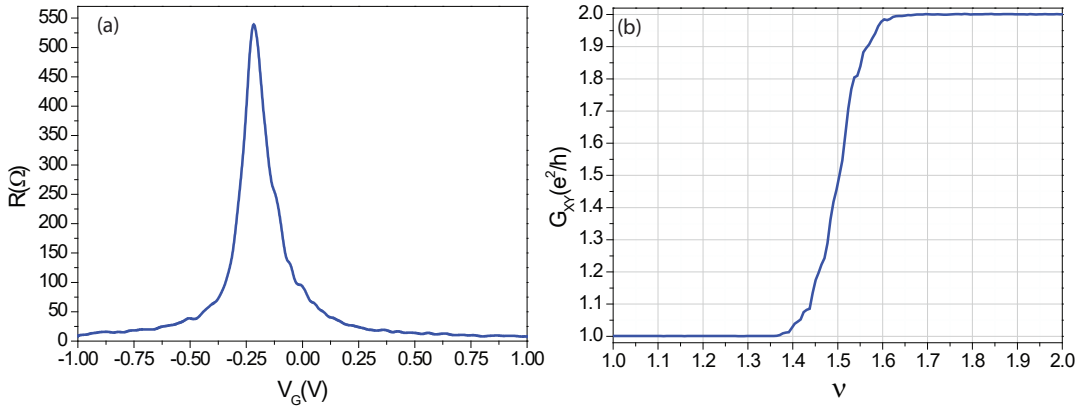

FIG. S1. (a) Plot of R vs V_G measured at T=20mK, in Device B15D4. (b) Plot of the quantum Hall $\nu = 1$ to $\nu = 2$ transition obtained at T=20mK, B=16T – ν is tuned by sweeping the gate voltage.

Appendix B: Analysis of multifractality

We explain the analysis of the conductance fluctuations to obtain the multifractal spectrum in this supplementary material. Fig. S2(a) shows the plot of conductance G_{XY} versus ν for the quantum Hall plateaus $\nu = 1$ to $\nu = 2$ transition (blue line). The fluctuations observed have been confirmed to be mesoscopic fluctuations, as mentioned in the main paper. The background is marked by the solid orange line, obtained by averaging over the data. On subtracting the background, we obtain the conductance fluctuations G'_{XY} as shown in Fig. S2(b).

We divide G'_{XY} versus ν data into overlapping segments, centered at different ν with a fixed span in ν for further analysis. This center value of ν for each such segment is used to label the multifractal spectrum of that given data set. To give an example, the multifractal spectrum in Fig. 3(b-c) in the main text is the spectrum for such a dataset of G'_{XY} versus ν centered at $\nu = 1.47$. We now explain, in brief, the method to obtain multifractal singularity spectrum for each such dataset.

We carry out the data analysis using the multifractal detrended fluctuation analysis (MFDFA) method [49].

1. The dataset is divided into N_s overlapping segments (indexed by j) with s data points each; $\{g_i\}$, $i = 1, 2, ..., s$.

2. From each N_s segment, local trend is removed by fitting a polynomial to the data. We have used a polynomial of order 1 to treat our data. Then we obtain the variance for each such segment:

$$g_{rms}(j) = \left[\frac{1}{s}\sum_{i=1}^{s}(g_i)^2\right]^{1/2}. \tag{B1}$$

3. The order-q moment of the fluctuations $F_q(s)$ is obtained:

$$F_q(s) = \left[\frac{1}{N_s}\sum_{j=1}^{N_s} g_{rms}(j)^q\right]^{1/q}. \tag{B2}$$

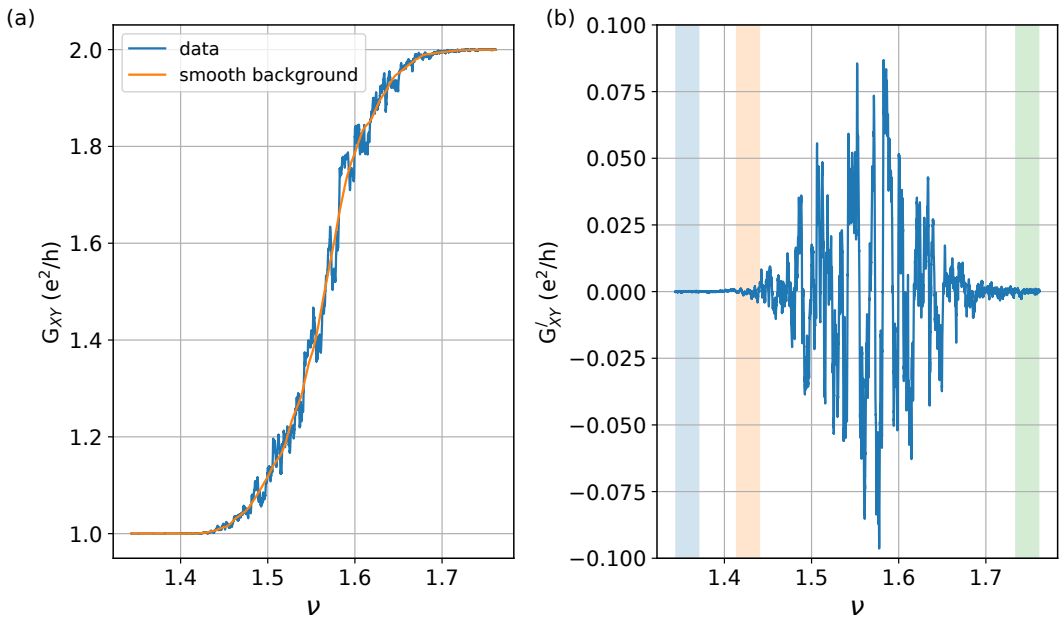

FIG. S2. (a) Representative plot of G_{XY}, in units of e^2/h versus ν for the quantum Hall plateaus $\nu = 1$ to $\nu = 2$ transition is shown. The blue line is the data, while the orange line is a smooth background, used to obtain the fluctuations in G_{XY}. (b) Plot of G'_{XY} versus ν obtained after subtracting the background. Standard deviation, in units of e^2/h, of the data were compared in the shaded regions - 1.24×10^{-4} and 5.66×10^{-4} obtained in blue and green shaded regions give an estimate of measurement noise level at plateau corresponding to $\nu = 1$ and $\nu = 2$ respectively. In contrast, the value 1.15×10^{-3} observed at the orange shaded region suggests that the fluctuations that we analyze are much larger than the measurement noise level. We also note that the orange region marks onset of the multifractal fluctuations.

4. The order-q moment of the fluctuations $F_q(s)$ scales with the segment size s with a power $h(q)$ as shown in Eqn. 3 of the main paper, and is known as the generalized Hurst exponent.

$$F_q(s) \sim s^{h(q)}. \tag{B3}$$

The scaling exponent is obtained from the slope of $\log(F_q(s))$ versus $\log(s)$ plot, for each values of q, and we obtain $h(q)$.

The spectrum $h(q)$ versus q characterizes the multifractality of a data series. Multifractality is conveniently represented using the singularity spectrum $f(\alpha)$ versus α which is defined as:

$$\tau(q) = h(q)q - 1$$

The singularity spectrum is related to $\tau(q)$ via a Legendre transform:

$$\alpha = \frac{d\tau(q)}{dq}$$
$$f(\alpha) = q\alpha - \tau(q).$$

The spectral width $\Delta\alpha$ quantifies the multifractality of the data.

Appendix C: Multifractality at different magnetic fields

Fig. S3 is a plot of the multifractal spectral width $\Delta\alpha$ versus ν, measured at different magnetic fields $B = 16.0$ T, $B = 10.0$ T, and $B = 6.0$ T. Having different magnetic fields at a fixed ν corresponds to different charge carrier densities ($\nu = nh/eB$). We observe that there is no visible effect of the charge carrier density or the magnetic field on the multifractal spectral width – $\Delta\alpha$ depends only on ν.

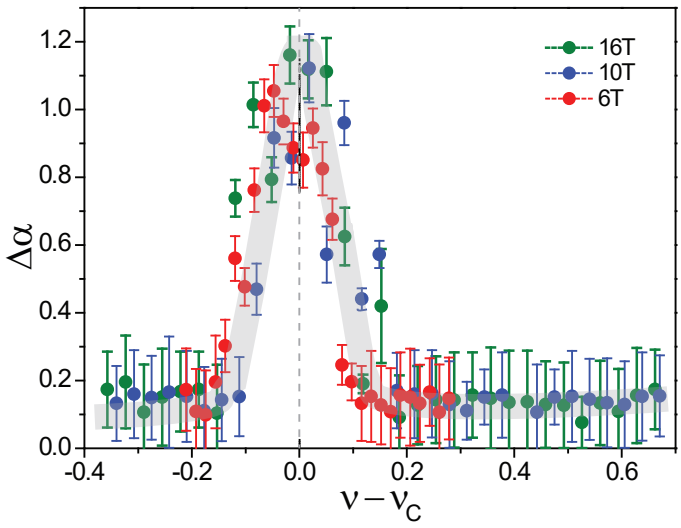

FIG. S3. Plot of $\Delta\alpha$ versus $\nu - \nu_C$, where ν_C is the critical point for $\nu = 1$ to $\nu = 2$ transition. Data were measured at $B = 16.0$ T (green filled circles), $B = 10.0$ T (blue filled circles) and $B = 6.0$ T (red filled circles).

* aveek@iisc.ac.in

[1] S. Girvin and R. Prange, eds., *The quantum Hall effect*.

[2] K. v. Klitzing, G. Dorda, and M. Pepper, New method for high-accuracy determination of the fine-structure constant based on quantized hall resistance, Phys. Rev. Lett. **45**, 494 (1980).

[3] J. E. Avron, R. Seiler, and B. Simon, Charge deficiency, charge transport and comparison of dimensions, Communications in mathematical physics **159**, 399 (1994).

[4] D. J. Thouless, M. Kohmoto, M. P. Nightingale, and M. den Nijs, Quantized hall conductance in a two-dimensional periodic potential, Physical review letters **49**, 405 (1982).

[5] J. Bellissard, A. van Elst, and H. Schulz-Baldes, The noncommutative geometry of the quantum hall effect, Journal of Mathematical Physics **35**, 5373 (1994).

[6] J. E. Avron, D. Osadchy, and R. Seiler, A topological look at the quantum hall effect, Physics today **56**, 38 (2003).

[7] B. Huckestein, Scaling theory of the integer quantum hall effect, Reviews of Modern Physics **67**, 357 (1995).

[8] W. Li, C. Vicente, J. Xia, W. Pan, D. Tsui, L. Pfeiffer, and K. West, Scaling in plateau-to-plateau transition: a direct connection of quantum hall systems with the anderson localization model, Physical review letters **102**, 216801 (2009).

[9] J. Chalker, The integer quantum hall effect and anderson localisation, in *Aspects topologiques de la physique en basse dimension. Topological aspects of low dimensional systems* (Springer, 1999) pp. 879–893.

[10] J. Chalker and G. Daniell, Scaling, diffusion, and the integer quantized hall effect, Physical review letters **61**, 593 (1988).

[11] B. Huckestein and B. Kramer, One-parameter scaling in the lowest landau band: Precise determination of the critical behavior of the localization length, Physical review letters **64**, 1437 (1990).

[12] B. Huckestein and L. Schweitzer, Multifractal behavior and scaling in disordered mesoscopic qhe-systems, Physica A: Statistical Mechanics and its Applications **191**, 406 (1992).

[13] B. Huckestein and L. Schweitzer, Relation between the correlation dimensions of multifractal wave functions and spectral measures in integer quantum hall systems, Physical review letters **72**, 713 (1994).

[14] K. R. Amin, S. S. Ray, N. Pal, R. Pandit, and A. Bid, Exotic multifractal conductance fluctuations in graphene, Communications Physics **1**, 1 (2018).

[15] G. Benenti, G. Casati, I. Guarneri, and M. Terraneo, Quantum fractal fluctuations, Physical review letters **87**, 014101 (2001).

[16] G. Casati, I. Guarneri, and G. Maspero, Fractal survival probability fluctuations, Physical review letters **84**, 63 (2000).

[17] A. Facchini, S. Wimberger, and A. Tomadin, Multifractal fluctuations in the survival probability of an open quantum system, Physica A: Statistical Mechanics and its Applications **376**, 266 (2007).

[18] A. Espinosa-Champo and G. G. Naumis, Multifractal wavefunctions of charge carriers in graphene with folded deformations, ripples, or uniaxial flexural modes: Analogies to the quantum hall effect under random pseudomagnetic fields, Journal of Vacuum Science & Technology B **39**, 062202 (2021), https://doi.org/10.1116/6.0001337.

[19] A. Tsinober, Turbulence: The legacy of an kolmogorov. by u. frisch. cambridge university press, 1995. 296 pp. isbn 0 521 45713 0.£ 15.95., Journal of Fluid Mechanics **317**, 407 (1996).

[20] M. Ghil, R. Benzi, and G. Parisi, *Turbulence and predictability in geophysical fluid dynamics and climate dynamics*, Vol. 88 (North Holland, 1985).

[21] R. Benzi, G. Paladin, G. Parisi, and A. Vulpiani, On the multifractal nature of fully developed turbulence and chaotic systems, Journal of Physics A: Mathematical and General **17**, 3521 (1984).

[22] R. Pandit, P. Perlekar, and S. S. Ray, Statistical properties of turbulence: an overview, Pramana **73**, 157 (2009).

[23] N. Pal, P. Perlekar, A. Gupta, and R. Pandit, Binary-fluid turbulence: Signatures of multifractal droplet dynamics and dissipation reduction, Physical Review E **93**, 063115 (2016).

[24] S. Buldyrev, N. Dokholyan, A. Goldberger, S. Havlin, C.-K. Peng, H. Stanley, and G. Viswanathan, Analysis of dna sequences using methods of statistical physics, Physica A: Statistical Mechanics and its Applications **249**, 430 (1998).

[25] M. Zeng, X.-N. Zhang, J.-H. Li, and Q.-H. Meng, The scaling properties of high-frequency wind speed records based on multiscale multifractal analysis., Acta Physica Polonica B **47** (2016).

[26] S. Bhattacharjee, R. Pandit, T. Vesala, I. Mammarella, G. Katul, and G. Sahoo, Anisotropy and multifractal analysis of turbulent velocity and temperature in the roughness sublayer of a forested canopy, arXiv preprint arXiv:2010.04194 (2020).

[27] R. Mantegna and H. Stanley, An introduction to econophysics: Correlations and complexity in finance, Nature **53** (2000).

[28] J. Gieraltowski, J. Zebrowski, and R. Baranowski, Multiscale multifractal analysis of heart rate variability recordings with a large number of occurrences of arrhythmia, Physical Review E **85**, 021915 (2012).

[29] P. C. Ivanov, L. A. N. Amaral, A. L. Goldberger, S. Havlin, M. G. Rosenblum, Z. R. Struzik, and H. E. Stanley, Multifractality in human heartbeat dynamics, Nature **399**, 461 (1999).

[30] K. Ivanova, M. Ausloos, E. Clothiaux, and T. Ackerman, Break-up of stratus cloud structure predicted from non-brownian motion liquid water and brightness temperature fluctuations, Europhysics Letters **52**, 40 (2000).

[31] J. Sutradhar, S. Mukerjee, R. Pandit, and S. Banerjee, Transport, multifractality, and the breakdown of single-parameter scaling at the localization transition in quasiperiodic systems, Physical Review B **99**, 224204 (2019).

[32] B. Jack, F. Zinser, E. J. Konig, S. N. Wissing, A. B. Schmidt, M. Donath, K. Kern, and C. R. Ast, Visualizing the multifractal wave functions of a disordered two-dimensional electron gas, Physical Review Research **3**, 013022 (2021).

[33] J. Barrios-Vargas and G. G. Naumis, Electron localization in disordered graphene for nanoscale lattice sizes: multifractal properties of the wavefunctions, 2D Materials **1**, 011009 (2014).

[34] L. G. C. S. Sá, A. L. R. Barbosa, and J. G. G. S. Ramos, Conductance peak density in disordered graphene topological insulators, Phys. Rev. B **102**, 115105 (2020).

[35] N. L. Pessoa, A. L. R. Barbosa, G. L. Vasconcelos, and A. M. S. Macedo, Multifractal magnetoconductance fluctuations in mesoscopic systems, Phys. Rev. E **104**, 054129 (2021).

[36] C. Rubio-Verdu, A. M. Garcia-Garcia, H. Ryu, D.-J. Choi, J. Zaldivar, S. Tang, B. Fan, Z.-X. Shen, S.-K. Mo, J. I. Pascual, *et al.*, Visualization of multifractal superconductivity in a two-dimensional transition metal dichalcogenide in the weak-disorder regime, Nano letters **20**, 5111 (2020).

[37] X. Zhang, K.-T. Tsai, Z. Zhu, W. Ren, Y. Luo, S. Carr, M. Luskin, E. Kaxiras, and K. Wang, Correlated insulating states and transport signature of superconductivity in twisted trilayer graphene superlattices, Phys. Rev. Lett. **127**, 166802 (2021).

[38] L. Ponomarenko, A. Geim, A. Zhukov, R. Jalil, S. Morozov, K. Novoselov, I. Grigorieva, E. Hill, V. Cheianov, V. FalKo, *et al.*, Tunable metal–insulator transition in double-layer graphene heterostructures, Nature Physics **7**, 958 (2011).

[39] S. D. Sarma, S. Adam, E. Hwang, and E. Rossi, Electronic transport in two-dimensional graphene, Reviews of modern physics **83**, 407 (2011).

[40] A. Kou, B. E. Feldman, A. J. Levin, B. I. Halperin, K. Watanabe, T. Taniguchi, and A. Yacoby, Electron-hole asymmetric integer and fractional quantum hall effect in bilayer graphene, Science **345**, 55 (2014).

[41] M. Janssen, Multifractal analysis of broadly-distributed observables at criticality, International Journal of Modern Physics B **8**, 943 (1994).

[42] D. Polyakov, Quantum hall effect at finite temperatures, arXiv preprint cond-mat/9608013 (1996).

[43] D. H. Cobden, C. Barnes, and C. Ford, Fluctuations and evidence for charging in the quantum hall effect, Physical review letters **82**, 4695 (1999).

[44] B. E. Feldman, B. Krauss, J. H. Smet, and A. Yacoby, Unconventional sequence of fractional quantum hall states in suspended graphene, Science **337**, 1196 (2012).

[45] S. Ilani, J. Martin, E. Teitelbaum, J. Smet, D. Mahalu, V. Umansky, and A. Yacoby, The microscopic nature of localization in the quantum hall effect, Nature **427**, 328 (2004).

[46] E. Peled, D. Shahar, Y. Chen, D. Sivco, and A. Cho, Observation of a quantized hall resistivity in the presence of mesoscopic fluctuations, Physical review letters **90**, 246802 (2003).

[47] E. Peled, D. Shahar, Y. Chen, E. Diez, D. Sivco, and A. Cho, Near-perfect correlation of the resistance components of mesoscopic samples at the quantum hall regime, Physical review letters **91**, 236802 (2003).

[48] D. Cobden and E. Kogan, Measurement of the conductance distribution function at a quantum hall transition, Physical Review B **54**, R17316 (1996).

[49] R. A. Meyers, *Mathematics of complexity and dynamical systems* (Springer Science & Business Media, 2011).